AIAA JOURNAL
Vol. 46, No. 3, March 2008

Design-Oriented Thermostructural Analysis with External and Internal Radiation, Part 1: Steady State

Manav Bhatia* and Eli Livne†
University of Washington, Seattle, Washington 98195-2400

DOI: 10.2514/1.26236

This paper presents a steady-state sensitivity analysis formulation covering configuration shape and structural sizing design variables for coupled linear structural analysis and nonlinear thermal analysis including the effects of radiation: in external and internal cavities. A new coupled design-oriented thermoelastic analysis capability is first presented and validated by using an available commercial analysis code. It is then used to calculate shape sensitivities and assess a number of standard approximation techniques in an effort to gain insight regarding the functional relations between design variables and thermoelastic responses. A novel approximation scheme is presented for the category of problems discussed that lead to substantial savings in central processing unit time. A hypersonic wing structure similar to a space shuttle wing is used as a test case.

Nomenclature

A_i	=	any area in three-dimensional space describing a surface participating in heat exchange through radiation
$[B]$	=	strain operator matrix
AR	=	wing aspect ratio
c_{root}	=	wing root chord
c_{tip}	=	wing tip chord
dA_i	=	infinitesimal surface area on A_i
$\{F_B\}$	=	load vector due to distributed body forces
$\{F_C\}$	=	load vector due to surface tranction
F_{i-j}	=	shape factor from finite surface A_i to another finite surface A_j
$[F_{i-j}]$	=	matrix of shape factors in cavity radiation analysis
$\{F_N\}$	=	load vector due to concentrated nodal forces
$\{F_T\}$	=	load vector due to temperature distribution
$\{F_u\}$	=	nodal reactions at nodes with displacement boundary conditions
h	=	coefficient of surface heat convection
$[J]$	=	Jacobian of the heat-transfer finite element equations
$[K]$	=	structural stiffness matrix
$[K_C]$	=	thermal conductivity matrix for the structure
$[K_h]$	=	conductance matrix resulting from surface convection
k_i	=	coefficient of thermal heat conduction in x_i direction
$\{N\}$	=	vector of finite element shape functions
n_i	=	surface normal describing A_i
q	=	net heat flux flowing out of a radiation surface
q_{fe}	=	input flux on finite element grid points
q_i	=	heat flux in the x_i direction due to conduction or incident heat flux due to irradiation
q_{rad}	=	incoming radiant flux vector for the cavity radiation analysis
q_s	=	surface heat flux
q_v	=	internal volume heat generation
q_o	=	radiation heat flux leaving a surface
$\{R_h\}$	=	load vector due to surface convection
$\{R_Q\}$	=	load vector due to internal heat generation
$\{R_q\}$	=	load vector due to applied surface heat flux
$\{R_T\}$	=	nodal heat loads at nodes with temperature boundary conditions
$\{R_\sigma\}$	=	load vector due to radiation
S	=	magnitude of S_{ij}
S_{ij}	=	vector from centroid of surface A_i to A_j
T	=	temperature variable
$\{T\}$	=	finite element nodal temperature vector
T_{abs}	=	absolute temperature scale, 273.16 K
t_{wing}	=	wing depth
$\{T_{\text{rad}}\}$	=	temperature of the surfaces participating in the internal cavity radiation exchange
T_0	=	structural reference temperature for calculation of thermal load
T_∞	=	ambient temperature
$\{u\}$	=	structural displacement vector
$\{\tilde{u}\}$	=	nodal displacement vector for a finite element
X	=	design variable
α	=	surface absorptivity or coefficient of thermal expansion for thermoelastic analysis
Γ	=	boundary of finite element
ΔT	=	temperature difference with respect to T_0 for thermal loads on a structure
ϵ	=	surface emissivity
$\{\epsilon\}$	=	strain vector
θ_i	=	angle between the n_i and S_{ij}
Λ_{LE}	=	wing leading-edge sweep angle
ρ	=	material density
σ	=	Stefan–Boltzmann constant
σ_{ij}	=	stress tensor
$\{\sigma\}$	=	stress vector
Ω	=	volume of finite element
$[\,]_{\text{diag}}$	=	diagonal matrix

Subscripts

i, j	=	row and column index

Introduction

THE coupling of thermal-structural simulations for aerospace vehicles is one of the key elements of any multidisciplinary design optimization (MDO) capability for such vehicles. The problem is computationally challenging and requires detailed large-scale

Presented as Paper 2054 at the 47th AIAA/ASME/ASCE/AHS/ASC Structures, Structural Dynamics, and Materials Conference, Newport, RI, 1–4 May 2006; received 28 June 2006; revision received 23 September 2007; accepted for publication 23 September 2007.

*Ph.D. Student, Department of Aeronautics and Astronautics, Box 352400. Member AIAA.

†Professor, Department of Aeronautics and Astronautics, Box 352400. Associate Fellow AIAA.

finite element (FE) structural and thermal models, different meshes tailored to simulation needs in each of the disciplines, information transfer between the meshes, and, in the case of design-oriented analysis (DOA), automated model generation and behavior sensitivity information. That, in turn, is used to generate approximate behavior results: the key to the practicality and success of any nonlinear programming/approximation concepts (NLP/AC) strategy to MDO.

Although publications describing contributions to thermal-structural analysis are abundant, the design-oriented thermo-structural analysis capable of modeling real aerospace vehicles is still a challenging problem. Ko et al. studied the thermal [1,2] and thermoelastic [3] response of an actual orbiter structure during the reentry phase. They accounted for external heat loads and internal cavity radiation analysis. They obtained temperature and stress predictions, which were in good agreement with in-flight measured data.

Ko et al. [4] evaluated the importance of incorporating effects of heat transfer through internal radiation and convection inside the cavities of the structure. They found out that for structures like the orbiter wing box, modeling internal radiation is critical to the accuracy of the thermal response simulation during the reentry phase. Internal convection, on the other hand, needs to be modeled after touchdown when all vents are opened to facilitate forced convective cooling of the structure.

For sensitivity analysis of thermoelastic problems, Meric [5–7] and Tortorelli et al. [8,9] presented work based on variational formulations. Meric [5–7] used the material derivative approach for shape sensitivity analysis, and Tortorelli et al. [8,9] used the domain parametrization approach with linear transient heat transfer and nonlinear structural response. Recently, Dems and Korycki [10] presented the sensitivity analysis for a nonlinear heat conduction problem with internal cavity radiation exchange inside the structure. He used boundary elements to solve the problem of internal radiation. This approach, however, results in complex equations for sensitivity analysis requiring a major programming effort.

Gu et al. [11,12] used the discrete semi-analytic method [13] for thermoelastic shape sensitivity analysis with nonlinear heat transfer. Chen et al. [14] performed sensitivity analysis for thermoelastic problems with thermally induced vibrations. Xu and Grandhi [15] used a two-point approximation with sensitivity analysis of thermal and structural quantities.

Overall, the semi-analytic shape sensitivity analysis formulation for a heat transfer problem including internal radiation and conduction has not been studied in the literature. This paper presents this formulation using finite element discretization for heat conduction analysis and structural analysis, and Poljak's discretization method for internal radiation analysis. A methodology is presented for the coupling of these analysis methods. It is assumed, at this stage of development of the technology, that structural displacements and stresses do not affect the temperature field.

Because the generation of radiation shape factors is a major consumer of computational effort in problems with internal and external radiation when the shape of a structure changes during shape optimization, a new approximate technique is presented here based on approximating the shape-factor matrix as an intermediate quantity. It is shown that this approximation method can lead to significant reduction in CPU time with much better results compared with conventional approximation methods such as direct and reciprocal approximation.

A newly developed finite element code (FESystem) is used to perform analysis and sensitivity analysis for this coupled problem. The results presented here are generated using FESystem, which is written in C++ with an object-oriented design. It uses libMesh [16] for handling the finite element mesh and its sparsity pattern and for calculation of finite element shape functions and their derivatives. PETSc [17,18] is used as the solver. The focus of this paper is on the steady-state problem, with extensions to transient problems discussed in a subsequent paper.

Fundamental Equations

Heat Transfer

The governing differential equation for the steady-state heat transfer problem is written as

$$q_{i,i} - q_v = 0 \qquad i = 1, 2, 3 \tag{1}$$

where ρ = material density, q_i = tensor representation of heat flux, and q_v = internal volume heat generation. Fourier's law of heat conduction defines the heat flux as

$$q_i = -k_i T_{,i} \tag{2}$$

where k_i is the coefficient of thermal conductivity, and a comma in the subscript indicates differentiation with respect to the ith spacial coordinate. Boundary conditions for this differential equation can be of the following form:

$$T = T_s \text{ temperature boundary condition on } S_1$$

$$q = q_s \text{ surface heat flux on } S_2$$

$$q = -h(T - T_\infty) \text{ surface heat convection on } S_3$$

$$q = -\sigma\epsilon T^4 \text{ emitted radiation on } S_4$$

and

$$q = \alpha q_R \text{ absorbed radiation on } S_4$$

where S_i belong to the boundary of the domain.

The discretized finite element equation of steady-state conduction heat transfer is written as Eq. (3) [19]:

$$[[K_c] + [K_h]]\{T\} = \{R_T\} + \{R_Q\} + \{R_q\} + \{R_h\} + \{R_\sigma\} \tag{3}$$

where

$$[K_c] = \int_\Omega (\{N\}_{,i} k_i \{N\}_{,i}^T)\, \mathrm{d}\Omega \tag{4}$$

$$[K_h] = \int_{S_3} h\{N\}\{N\}^T\, \mathrm{d}\Gamma \tag{5}$$

$$\{R_T\} = -\int_{S_1} (\boldsymbol{q} \cdot \hat{n})\{N\}\, \mathrm{d}\Gamma \tag{6}$$

$$\{R_Q\} = \int_\Omega q_v\{N\}\, \mathrm{d}\Omega \tag{7}$$

$$\{R_q\} = \int_{S_2} q_s\{N\}\, \mathrm{d}\Gamma \tag{8}$$

$$\{R_h\} = \int_{S_3} hT_\infty\{N\}\, \mathrm{d}\Gamma \tag{9}$$

$$\{R_\sigma\} = -\int_{S_4} \sigma[\epsilon(T + T_{\text{abs}})^4 - \alpha(T_{\text{amb}} + T_{\text{abs}})^4]\{N\}\, \mathrm{d}\Gamma \tag{10}$$

The radiation load $\{R_\sigma\}$ is nonlinear in nature and is dependent on the fourth power of temperature. Solution of the system of nonlinear equations [Eq. (3)] requires calculation of the Jacobian matrix, which is defined as

$$[J] = \frac{\partial}{\partial T}[([K_C] + [K_h])\{T\} - (\{R_Q\} + \{R_q\} + \{R_h\} + \{R_\sigma\})]$$
$$= -\int_{S_4} 4\sigma\epsilon\{N\}(T + T_{\text{abs}})^3\{N\}^T \, \mathrm{d}\Gamma \tag{11}$$

A method for calculating the net heat flux exchange on boundary S_4 participating in cavity radiation is described in the next section.

Sensitivity Analysis

To obtain the sensitivity of the nodal temperatures, Eq. (3) can be implicitly differentiated [20] to obtain

$$[J]\frac{\partial\{T\}}{\partial X} = \frac{\partial\{p\}}{\partial X} - \frac{\partial\{f\}}{\partial X} \tag{12}$$

where

$$\frac{\partial p}{\partial X} = \frac{\partial}{\partial X}(\{R_Q\} + \{R_q\} + \{R_h\} + \{R_\sigma\}) \tag{13}$$

$$\frac{\partial f}{\partial X} = \frac{\partial}{\partial X}([K_C] + [K_h])\{T\} \tag{14}$$

Here, $[J]$ is the Jacobian of the nonlinear heat transfer problem [Eq. (11)] calculated at the point of thermal equilibrium; in other words, it is calculated using the solution of Eq. (3). If Newton's method is used to solve Eq. (11), $[J]$ is available from its final iteration.

For the case in which internal cavity radiation is included, the sensitivity of the incident radiation flux is calculated as shown in the next subsection.

Cavity Radiation

The following assumptions are introduced for analysis of cavity radiation:

1) Surfaces are gray and diffusely emitting and reflecting.

2) Surfaces are isothermal.

Because of the assumption of gray surfaces, we get the following relation between emissivity ϵ, reflectivity ρ, and absorptivity α of the surface:

$$\epsilon = \alpha = 1 - \rho \tag{15}$$

Using the assumption of diffuse emission, the energy exchange between two surfaces can be calculated using shape factors. The radiation shape factor from surface i to j is defined as the fraction of energy leaving surface i and directly received by surface j (Fig. 1) , and is represented as

$$F_{i-j} = \frac{1}{A_i}\int_{A_i}\int_{A_j} \frac{\cos\theta_i \cos\theta_j}{\pi S^2} \, \mathrm{d}A_j \, \mathrm{d}A_i \tag{16}$$

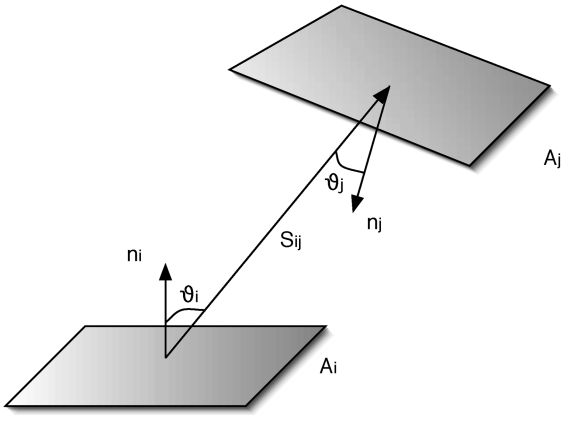

Fig. 1 Geometry for shape-factor calculation.

where $\mathrm{d}A_i$ and $\mathrm{d}A_j$ = elemental surface areas on A_i and A_j, θ_i = angle between the surface normal for $\mathrm{d}A_i$ and the vector from $\mathrm{d}A_i$ to $\mathrm{d}A_j$, θ_j = angle between the surface normal for $\mathrm{d}A_j$ and the vector from $\mathrm{d}A_j$ to $\mathrm{d}A_i$, and S = magnitude of the vector from $\mathrm{d}A_i$ to $\mathrm{d}A_j$.

Calculation of Shape Factors

For a cavity with N surfaces, the number of unobstructed shape factors to be calculated is on the order of N^2. If obstructions are taken into account, the order increases to N^3. Walton [21] presents an overview of the shape-factor calculation methods, and goes on to describe an adaptive algorithm for calculation of obstructed shape factors. In general, the methods are based on numerical integration and are limited in applicability for cases in which two surfaces share a common edge. Schroder and Hanrahan [22] established a closed-form solution for calculation of shape factors between polygons.

In the work described in the paper, it is assumed that there is no shadowing involved in the calculation of the shape factors. Internal cavities are assumed to be convex in shape with all face elements exchanging radiation. Shape factors have been calculated using the solutions of Schroder and Hanrahan [22].

Poljak's Method

Radiation heat exchange inside a cavity of gray surfaces can be analyzed using Poljak's method [23]. If surfaces are assumed to be isothermal, the balance of heat flux for each surface can be written as

$$\{q\} = \{q_o\} - \{q_i\} \tag{17}$$

where

$$\{q_o\} = \sigma[\epsilon]\{T^4\} + [\rho]\{q_i\} = \sigma[\epsilon]\{T^4\} + [1 - \epsilon]\{q_i\} \tag{18}$$

The incident flux on surface k is expressed as

$$A_k q_{i,k} = \sum_{j=1}^{N} q_{o,j} A_j F_{k-j} \tag{19}$$

where A_k is the area of the kth surface. Using the reciprocity relation for shape factors

$$A_k F_{j-k} = A_j F_{k-j} \tag{20}$$

we can rewrite $q_{i,k}$ as

$$A_k q_{i,k} = A_k \sum_{j=1}^{N} q_{o,j} F_{j-k} \tag{21}$$

or

$$q_{i,k} = \sum_{j=1}^{N} q_{o,j} F_{j-k} \tag{22}$$

In matrix notation, this can be written as

$$\{q_i\} = [F_{j-k}]\{q_o\} \tag{23}$$

For a set of n radiation surfaces with specified temperatures, Eqs. (17), (18), and (23) form a set of $3n$ equations with $3n$ unknowns: $\{q_i\}$, $\{q_o\}$, and $\{q\}$. These can be written in a matrix form as

$$\begin{bmatrix} [I] & [I] & -[I] \\ 0 & [I] & -[F_{i-j}] \\ 0 & [\epsilon - 1]_{\text{diag}} & [I] \end{bmatrix} \begin{Bmatrix} \{q\} \\ \{q_i\} \\ \{q_o\} \end{Bmatrix} = \begin{Bmatrix} 0 \\ 0 \\ \sigma[\epsilon]_{\text{diag}}\{T^4\} \end{Bmatrix} \tag{24}$$

Equation (24) can be solved to get

$$\begin{Bmatrix} \{q\} \\ \{q_i\} \\ \{q_o\} \end{Bmatrix} = \begin{Bmatrix} [A][B]^{-1}\{T^4\} \\ \sigma[F_{i-j}][B]^{-1}\{T^4\} \\ \sigma[B]^{-1}\{T^4\} \end{Bmatrix} \tag{25}$$

where

$$[A] = \sigma[[I] - [F_{i-j}]] \tag{26}$$

$$[B] = \left[\left[\frac{1}{\epsilon}\right]_{\text{diag}} - \left[\frac{1-\epsilon}{\epsilon}\right]_{\text{diag}}[F_{i-j}]\right] \tag{27}$$

Combined Finite Element and Internal Radiation Analysis

For a finite element analysis, the net thermal load on the nodes is the quantity of interest, which is defined by $-\{q\}$ in the radiation analysis. (The minus sign has been used because the sign convention in a finite element analysis defines the incoming flux on a surface as a positive quantity, and radiation defines the outgoing flux as positive.) Equation (25) defines the relation between surface temperature $\{T^4\}$ and net radiant heat flux out of the radiation element face $\{q\}$. The radiation elements are assumed to be isothermal with a constant heat flux over their surface. The heat flux obtained from Poljak's method will act as boundary flux loads on the finite element model. However, because the radiation and finite element models have different meshes, the temperature and flux data have to be related between the two meshes. The following method is used for this purpose.

A radiation cavity is defined by specifying the enclosing element faces. Each face is then uniformly subdivided into a specified number of radiation elements. Hence, any radiation element will be a part of only one finite element face. It should be noted that greater number of subdivisions result in higher accuracy for cavity radiation analysis, however, it also increases the number of shape-factor calculations.

With this simplification, the finite element nodal temperatures can be related to the temperatures of the enclosed radiation elements. Let T_{rad_i} be the temperature of the ith radiation element, and $\{T_{\text{fe}}\}$ be the vector of nodal temperatures of the finite element containing the radiation element. Then, we can obtain T_{rad_i} by equating the radiation energy leaving the surface of radiation element i. The amount of radiative energy leaving the isothermal surface is

$$q_{\text{rad}_i} = \sigma\epsilon_i A_i (T_{\text{rad}_i} + T_{\text{abs}})^4 \tag{28}$$

We can calculate the same quantity using finite element nodal temperatures, as

$$q'_{\text{rad}_i} = \sigma\epsilon_i \int_{\Omega_i} (\{N\}^T\{T_{\text{fe}}\} + T_{\text{abs}})^4 \, \text{d}\Omega \tag{29}$$

where the integration is performed over the domain of the ith radiation element which lies inside the finite element. Because the two fluxes should be equal, we can write

$$q_{\text{rad}_i} = q'_{\text{rad}_i} \tag{30}$$

giving

$$(T_{\text{rad}_i} + T_{\text{abs}})^4 = \frac{1}{A_i}\int_{\Omega_i} (\{N\}^T\{T_{\text{fe}}\} + T_{\text{abs}})^4 \, \text{d}\Omega \tag{31}$$

Upon following a similar procedure for all radiation elements, we can write

$$\{(T_{\text{rad}} + T_{\text{abs}})^4\}_k = [A_i]^{-1}_{\text{diag}_k}\left\{\int_{\Omega_i} (\{N\}^T\{T_{\text{fe}}\}_k + T_{\text{abs}})^4 d\Omega\right\}_k \tag{32}$$

where $\{T^4_{\text{rad}}\}_k$ is the vector of temperatures of the radiation elements enclosed by finite element k.

Similarly, the radiation flux can be related to the finite element nodal heat load vector. The flux on the ith radiation element q_{rad_i} can be integrated over its domain Ω_i to obtain the finite element nodal load vector $\{q_{\text{fe}}\}$.

$$\{q_{\text{fe}}\}_i = \int_{\Omega_i} \{N\} q_{\text{rad}_i} \, \text{d}\Omega \tag{33}$$

where subscript i implies contribution due to ith radiation element. Then, the total nodal heat load can be obtained by summing up the contributions due to all the radiation elements, giving

$$\{q_{\text{fe}}\}_k = \left[\int_{\Omega_1} \{N\} q_{\text{rad}_1} \, \text{d}\Omega \int_{\text{rad}_2} \{N\} q_{\text{rad}_2} \, \text{d}\Omega \cdots \int_{\Omega_N} \{N\} q_{\text{rad}_N} \, \text{d}\Omega\right]_k$$
$$= [G]^T_k \{q_{\text{rad}}\}_k \tag{34}$$

where $[G]_k$ is the interpolation matrix defined for finite element k as

$$[G]_k = \begin{bmatrix} \int_{\Omega_1}\{N\}^T \, \text{d}\Omega \\ \int_{\Omega_2}\{N\}^T \, \text{d}\Omega \\ \vdots \\ \int_{\Omega_N}\{N\}^T \, \text{d}\Omega \end{bmatrix}_k \tag{35}$$

Using Eq. (32) and (34) for all finite elements in the cavity, we can relate the finite element nodal load vector $\{q_{\text{fe}}\}$ to nodal temperatures as

$$\{q_{\text{fe}_g}\} = [G_g]^T[A][B]^{-1}(\{T_{\text{rad}_g}\} + T_{\text{abs}})^4 \tag{36}$$

where the subscript g indicates that the matrices are assembled for the entire cavity representing each finite element participating in the analysis. The vector $\{q_{\text{fe}_g}\}$ is directly added to the finite element nodal heat load vector.

Contribution of this nonlinear load vector to the finite element Jacobian matrix can be calculated by the expression given in Eq. (37), which assumes temperature independent material properties:

$$\left[\frac{\text{d}\{q_{\text{fe}_g}\}}{\text{d}\{T_{\text{fe}_g}\}}\right] = [G_g]^T[A][B]^{-1}\left[\frac{\text{d}(\{T_{\text{rad}_g}\} + T_{\text{abs}})^4}{\text{d}\{T_{\text{fe}_g}\}}\right] \tag{37}$$

where

$$\left[\frac{\text{d}(\{T_{\text{rad}_g}\} + T_{\text{abs}})^4}{\text{d}\{T_{\text{fe}_g}\}}\right]$$
$$= [A_i]^{-1}_{\text{diag}}\left[\int_{\Omega_i} 4(\{N\}^T\{T_{\text{fe}}\} + T_{\text{abs}})^3\{N\}^T \, \text{d}\Omega\right] \tag{38}$$

As an illustration of the process, consider the mesh on a single finite element as shown in Fig. 2. It consists of a four-noded quadrilateral conduction finite element defined by the nodes G1, G2, G3, and G4. For cavity radiation calculations, this element has been subdivided into four radiation elements R1, R2, R3, R4, which are assumed to be isothermal. If we define

$$\{T_{\text{fe}}\} = \{T_{G1} \;\; T_{G2} \;\; T_{G3} \;\; T_{G4}\}^T \tag{39}$$

$$\{q_{\text{fe}}\} = \{q_{G1} \;\; q_{G2} \;\; q_{G3} \;\; q_{G4}\}^T \tag{40}$$

$$\{T_{\text{rad}}\} = \{T_{R1} \;\; T_{R2} \;\; T_{R3} \;\; T_{R4}\}^T \tag{41}$$

$$\{q_{\text{rad}}\} = \{q_{R1} \;\; q_{R2} \;\; q_{R3} \;\; q_{R4}\}^T \tag{42}$$

then we can relate the quantities by the following relations:

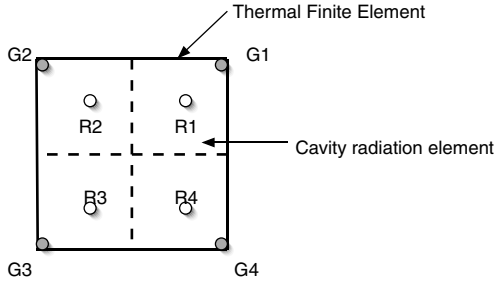

Fig. 2 Cavity radiation and finite element mesh.

$$[A_i]^{-1}_{\text{diag}} = \begin{bmatrix} 1/A_{R1} & & & \\ & 1/A_{R2} & & \\ & & 1/A_{R3} & \\ & & & 1/A_{R4} \end{bmatrix} \tag{43}$$

$$(\{T_{\text{rad}}\} + T_{\text{abs}})^4 = [A_i]^{-1}_{\text{diag}} \begin{Bmatrix} \int_{\Omega_{R1}} (\{N\}^T\{T_{\text{fe}}\} + T_{\text{abs}})^4 \, \mathrm{d}\Omega \\ \int_{\Omega_{R2}} (\{N\}^T\{T_{\text{fe}}\} + T_{\text{abs}})^4 \, \mathrm{d}\Omega \\ \int_{\Omega_{R3}} (\{N\}^T\{T_{\text{fe}}\} + T_{\text{abs}})^4 \, \mathrm{d}\Omega \\ \int_{\Omega_{R4}} (\{N\}^T\{T_{\text{fe}}\} + T_{\text{abs}})^4 \, \mathrm{d}\Omega \end{Bmatrix} \tag{44}$$

$$\{q_{\text{fe}}\} = \left[\int_{\Omega_{R1}} \{N\} \, \mathrm{d}\Omega \quad \int_{\Omega_{R2}} \{N\} \, \mathrm{d}\Omega \quad \int_{\Omega_{R3}} \{N\} \, \mathrm{d}\Omega \quad \int_{\Omega_{R4}} \{N\} \, \mathrm{d}\Omega \right] \{q_{\text{rad}}\} \tag{45}$$

$$\left[\frac{\mathrm{d}(\{T_{\text{rad}}\} + T_{\text{abs}})^4}{\mathrm{d}\{T_{\text{fe}}\}} \right] = [A_i]^{-1}_{\text{diag}} \begin{bmatrix} \int_{\Omega_{R1}} 4(\{N\}^T\{T_{\text{fe}}\} + T_{\text{abs}})^3 \{N\}^T \, \mathrm{d}\Omega \\ \int_{\Omega_{R2}} 4(\{N\}^T\{T_{\text{fe}}\} + T_{\text{abs}})^3 \{N\}^T \, \mathrm{d}\Omega \\ \int_{\Omega_{R3}} 4(\{N\}^T\{T_{\text{fe}}\} + T_{\text{abs}})^3 \{N\}^T \, \mathrm{d}\Omega \\ \int_{\Omega_{R4}} 4(\{N\}^T\{T_{\text{fe}}\} + T_{\text{abs}})^3 \{N\}^T \, \mathrm{d}\Omega \end{bmatrix} \tag{46}$$

Sensitivity Analysis

The expression for sensitivity of $\{q_{\text{fe}_g}\}$ with respect to a design variable X is obtained by implicit differentiation of Eq. (36).

$$\frac{\partial\{q_{\text{fe}_g}\}}{\partial X} = \frac{\partial([G_g]^T[A][B]^{-1}(\{T_{\text{rad}_g}\} + T_{\text{abs}})^4)}{\partial X} \tag{47}$$

If we introduce a new vector $\{\lambda\}$, so that

$$[B]\{\lambda\} = (\{T_{\text{rad}_g}\} + T_{\text{abs}})^4 \tag{48}$$

we can write the sensitivity as

$$\frac{\partial\{q_{\text{fe}_g}\}}{\partial X} = \frac{\partial([G_g]^T[A]\{\lambda\})}{\partial X} = \frac{\partial[G_g]^T}{\partial X}[A]\{\lambda\} + [G_g]^T\frac{\partial[A]}{\partial X}\{\lambda\} + [G_g]^T[A]\frac{\partial\{\lambda\}}{\partial X} \tag{49}$$

where the sensitivity of $\{\lambda\}$ can be calculated from Eq. (48) as

$$\frac{\partial\{\lambda\}}{\partial X} = [B]^{-1}\left(\frac{\partial\{(\{T_{\text{rad}_g}\} + T_{\text{abs}})^4\}}{\partial X} - \frac{\partial[B]}{\partial X}\{\lambda\} \right) \tag{50}$$

Here, the sensitivities of $[A]$ and $[B]$ are calculated as

$$\frac{\partial[A]}{\partial X} = \sigma\frac{\partial[F_{i-j}]}{\partial X} \tag{51}$$

$$\frac{\partial[B]}{\partial X} = \frac{\partial}{\partial X}\left(\left[\frac{1}{\epsilon}\right]_{\text{diag}} \right) - \frac{\partial}{\partial X}\left(\left[\frac{1-\epsilon}{\epsilon}\right]_{\text{diag}} \right)[F_{i-j}] - \left[\frac{1-\epsilon}{\epsilon}\right]_{\text{diag}}\frac{\partial[F_{i-j}]}{\partial X} \tag{52}$$

and the sensitivities of $[F_{i-j}]$, $[G_g]$, and $\{T_{\text{rad}_g}\}$ are calculated using finite differences. It must be noted that all quantities except for ϵ are dependent purely on geometry/shape and, hence, their sensitivities will be zero for a problem in which the design variable is a material parameter.

Structural Analysis

The structural finite element equations are given as in Eq. (53) [19]:

$$[K]\{u\} = \{F_u\} + \{F_c\} + \{F_B\} + \{F_T\} + \{F_N\} \tag{53}$$

where

$$[K] = \int_\Omega [B][C][B]^T \, \mathrm{d}\Omega \tag{54}$$

$$\{F_u\} = \int_{S_1} \{\sigma_{ij}\} \cdot \hat{n}\{N\} \, \mathrm{d}\Gamma \tag{55}$$

$$\{F_C\} = \int_{S_2} \{\sigma_{ij}\} \cdot \hat{n}\{N\} \, \mathrm{d}\Gamma \tag{56}$$

$$\{F_B\} = \int_\Omega \{B_F\}\{N\} \, \mathrm{d}\Gamma \tag{57}$$

$$\{F_T\} = \int_\Omega [B][C]\alpha\Delta T \, \mathrm{d}\Omega \tag{58}$$

Solution of Eq. (53) gives the nodal displacements over the discretized domain. The thermal load $\{F_T\}$ is calculated by integrating the temperature distribution ΔT over the domain of the structural element. Usually, temperature on the nodes of the structural elements is obtained from a thermal analysis, and ΔT is calculated using the expression

$$\Delta T = \{N\}^T\{T\} - T_0 \tag{59}$$

where $\{N\}$ are the shape functions of the structural finite element. The strains and stresses can be obtained from displacements using the strain operator $[B]$:

$$\{\epsilon\} = [B]\{\tilde{u}\} \tag{60}$$

and

$$\{\sigma\} = [C](\{\epsilon\} - \alpha\Delta T) = [C]([B]\{\tilde{u}\} - \alpha\Delta T) \tag{61}$$

Sensitivity Analysis

Similar to the heat transfer problem, Eq. (53) can be implicitly differentiated to obtain the equations for sensitivity of structural displacements given as

$$[K]\frac{\partial\{u\}}{\partial X} = \frac{\partial(\{F_u\} + \{F_c\} + \{F_B\} + \{F_T\} + \{F_N\})}{\partial X} - \frac{\partial[K]}{\partial X}\{u\} \tag{62}$$

The nodal temperatures and their sensitivities, which are obtained from the heat transfer analysis, are transferred from the thermal mesh to the structural nodes. Structural stresses and strains, and their sensitivities, can be calculated as

$$\frac{\partial\{\epsilon\}}{\partial X} = \frac{\partial[B]}{\partial X}\{\tilde{u}\} + [B]\frac{\partial\{\tilde{u}\}}{\partial X} \tag{63}$$

$$\frac{\partial\{\sigma\}}{\partial X} = \frac{\partial[C]}{\partial X}(\{\epsilon\} - \alpha\Delta T) + [C]\left(\frac{\partial\{\epsilon\}}{\partial X} - \frac{\partial\alpha}{\partial X}\Delta T - \alpha\frac{\partial\Delta T}{\partial X} \right) \tag{64}$$

Calculation of Sensitivity Quantities

The design variables considered here can be categorized into cross-sectional size, shape, and material variables. Because size and material parameters explicitly appear in the expressions for element quantities, analytic sensitivities with respect to them can be easily obtained. Sensitivity with respect to shape design variables are calculated using finite difference.

For example, sensitivity of the element heat conduction matrix $[K_c]$ [Eq. (4)] with respect to the material parameter k_i can be expressed as

$$\frac{\mathrm{d}[K_c]}{\mathrm{d}k_i} = \int_\Omega (\{N\}_{,i}\{N\}_{,i}^T \,\mathrm{d}\Omega \tag{65}$$

However, for a shape parameter α, the sensitivity is calculated using finite difference as

$$\left.\frac{\mathrm{d}[K_c]}{\mathrm{d}\alpha}\right|_{\alpha_0} = \frac{[K_c]|_{\alpha_1} - [K_c]|_{\alpha_0}}{\alpha_1 - \alpha_0} \tag{66}$$

where α_0 is the value of the design variable at which the sensitivity is to be calculated, and α_1 is the perturbed value of the design variable.

Sensitivity calculation of element load vectors is performed in a similar way, however, an additional load parameter needs to be accounted for in this process. For example, shape sensitivity of the element load vector due to volume heat generation in conduction analysis $\{R_Q\}$ is calculated as follows:

$$\left.\frac{\mathrm{d}\{R_Q\}}{\mathrm{d}\alpha}\right|_{\alpha_0} = \frac{(\int_\Omega \{N\}\,\mathrm{d}\Omega)|_{\alpha_1} - (\int_\Omega \{N\}\,\mathrm{d}\Omega)|_{\alpha_0}}{\alpha_1 - \alpha_0} q_v|_{\alpha_0} + \left(\int_\Omega \{N\}\,\mathrm{d}\Omega\right)\Bigg|_{\alpha_0} \frac{\mathrm{d}q_v}{\mathrm{d}\alpha} \tag{67}$$

Using this approach, all size and material sensitivities are calculated analytically and shape sensitivities are calculated semi-analytically.

Approximation

Calculation of the shape factors for radiation analysis is computationally demanding, especially when a large number of radiation elements are used. In the case of vehicle shape optimization, shape factors have to be calculated repeatedly for the changing shapes along the optimization path. If the full-order calculation of shape factors could be replaced by some fast approximate calculation, a considerable computational speedup would be achieved. With this insight, the shape factors are used as intermediate response functions (of shape) in the method presented here, and their variation with shape design variables is approximated using fast first-order Taylor approximations, i.e.,

$$[F]|_\alpha = [F]|_{\alpha_0} + \left.\frac{\partial[F]}{\partial\alpha}\right|_{\alpha_0} \Delta\alpha \tag{68}$$

The $[A]$ and $[B]$ matrices in Eqs. (26) and (27) are then calculated using the shape-factor matrix approximations (rather than *exactly* generated new shape factors by full integration) using Eq. (68). The shape-factor matrix is thus approximated, but the overall nonlinear analysis is still performed in full order.

In the following sections, performance of the new approximation is compared with performance of standard and computationally fast Taylor series approximations for the temperature, deformation, and stress responses. The Taylor series approximations are created using the following expressions [20]:

$$g(X)_{\text{linear}} = g(X_0) + \left.\frac{\mathrm{d}g(X)}{\mathrm{d}X}\right|_{X=X_0} (X - X_0) \tag{69}$$

$$g(X)_{\text{reciprocal}} = g(X_0) + \left.\frac{\mathrm{d}g(X)}{\mathrm{d}(1/X)}\right|_{X=X_0} \left(\frac{1}{X} - \frac{1}{X_0}\right) = g(X_0) + \left.\frac{\mathrm{d}g(X)}{\mathrm{d}X}\right|_{X=X_0} \left(\frac{X_0}{X}\right)(X - X_0) \tag{70}$$

The reciprocal approximation [20] is generated by replacing X, the actual design variable, by an intermediate design variable $Y = 1/X$, and expanding a constraint function or any response function $g(X)$ as a Taylor series in Y instead of X. In cases where the reciprocal approximation has a curvature opposite to that of the full-order analysis, a quadratic approximation may be generated by using an intermediate design variable $Y = X^2$. Such an approximation can be created (when X is substituted back into the resulting expression) to yield

$$g(X)_{\text{quad}} = g(X_0) + \left.\frac{\mathrm{d}g(X)}{\mathrm{d}X}\right|_{X=X_0} \frac{1}{2}\left(1 + \frac{X}{X_0}\right)(X - X_0) \tag{71}$$

In general, an intermediate design variable $Y = X^p$ can be used. It is impossible to know a priori, of course, what kind of an intermediate variable of such type will perform best in a first-order Taylor series of a particular response function. Some experimentation with the particular design variables and constraints in an optimization problem might offer some guidance here. Alternatively, a two-point or multiple-point approximation approach might be used, in which the coefficient p of intermediate design variables is calculated for each pair of design variable and response function. These might be obtained based on evaluation of Taylor series approximations in the intermediate variables at two or more points in the design space, as the optimization process progresses and multipoint exact information becomes available.

The purpose of the results shown here is not to promote one type of approximation or another but to draw attention to the different types of input–output (design variable–response function) dependencies possible in the coupled thermoelastic problem, where temperatures, deformations, and stresses respond differently to changes in shape or sizing design variables.

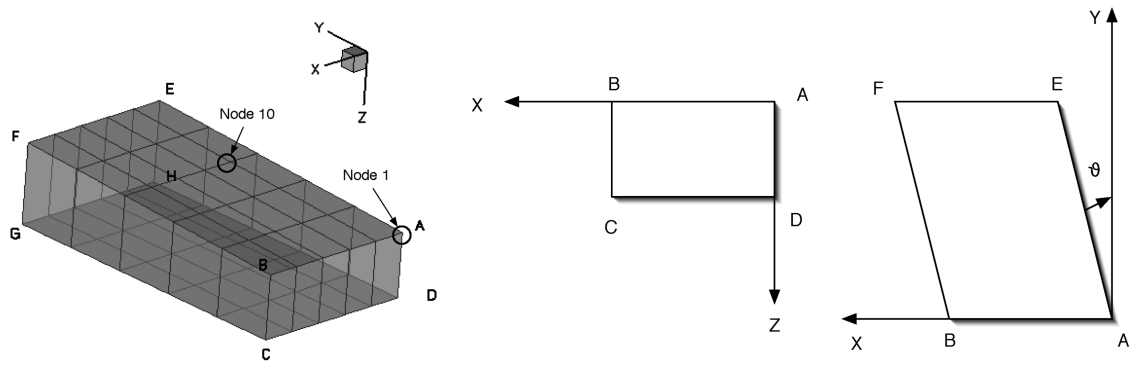

Fig. 3 Hexahedral cavity model.

Table 1 Material properties and size parameters

Parameter	Value
k_{skin}	190.0 W/m^2 · K
k_{TPS}	1.0 W/m^2 · K
ϵ_{skin}	0.65
ϵ_{TPS}	0.85
E_{skin}	70.0e9 Pa
ν_{skin}	0.33
α_{skin}	2.31e-5
t_{skin}	0.02 m
t_{TPS}	0.06 m
A_{caps}	1.0e-4

Results and Discussion

Hexahedral Radiating Cavity

The first shape studied here is a cavity shown in Fig. 3. A uniform heat load of 50 kW/m^2 is applied on the bottom surface, and both the bottom and top surfaces are allowed to radiate externally. Walls of the cavity are conducting and, inside the cavity, all surfaces exchange heat through radiation. The combined radiation conduction heat-transfer problem is solved using the approach described in the previous sections. Material properties with subscript "skin," as listed in Table 1, have been used in the finite element model.

Shape design variables studied for this example are the height of face ABCD and the shearing angle θ (see Fig. 3). Contour plots for temperature distribution are shown in Fig. 4. Figure 5 shows a parametric plot of temperature at nodes 1 and 10. As can be seen, internal radiation has a considerable effect on the temperature.

Sensitivity analysis, preformed at design variable values of 0.4 and 1.2, is used to create approximations to the temperature, as shown in Figs. 6–9. The reciprocal and quadratic approximations are both tangent to the full-order analysis curves at the point where the approximations are created. It is important to note in these figures that neither of these approximations provide a good fit to the full-order analysis curve over the range of the design variable. Hence, using these approximations in an approximation concepts-based optimization framework would need tight move limits, which would increase the overall number of full-order analyses required.

For Figs. 10 and 11, the shape-factor matrix was approximated using a linear Taylor series expansion about the reference point where exact analysis was carried out. The full-order nonlinear analysis was carried out with these approximated shape factors (and a saving in computing time). This approximation was studied for both of the aforementioned design variables. As can be seen from the figures, approximation of the shape-factor matrix using intermediate response functions provides a much better approximation than the standard Taylor series approximations of response functions.

It is also interesting to note from these plots that the accuracy of the approximation created at 0.4 is acceptable for a significantly smaller move limit than the approximation created at 1.2. The approximation created at 1.2 follows the full-order analysis quite well over a rather large range of design variable variation. This can be explained by considering Eq. (16), which shows that the shape factor between two areas is inversely proportional to the square of distance between them. As a result, the rate of change of F_{i-j} decreases as the surfaces move farther apart. A similar approximation for design variable θ (Fig. 12) provides a very good approximation to the full-order analysis and yields good accuracy over a wide range of design variable values.

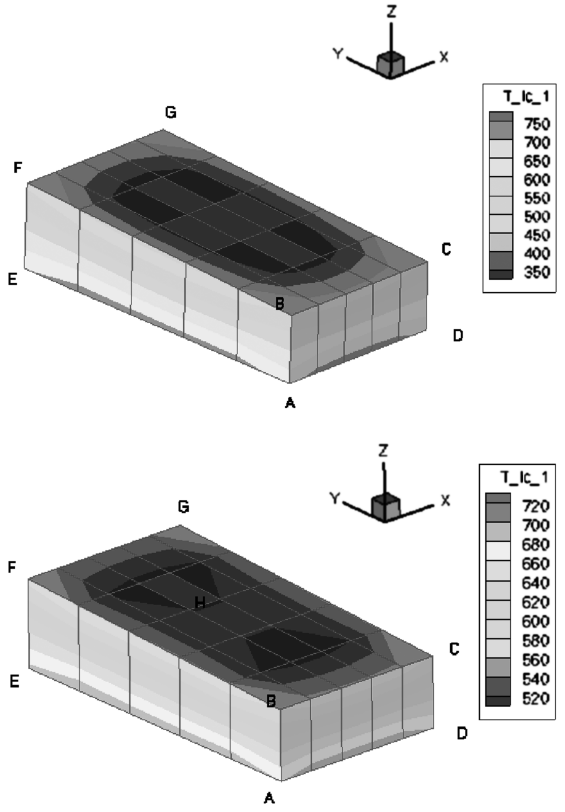

Fig. 4 Temperature contours with only external radiation (top), and both external and internal radiation (bottom).

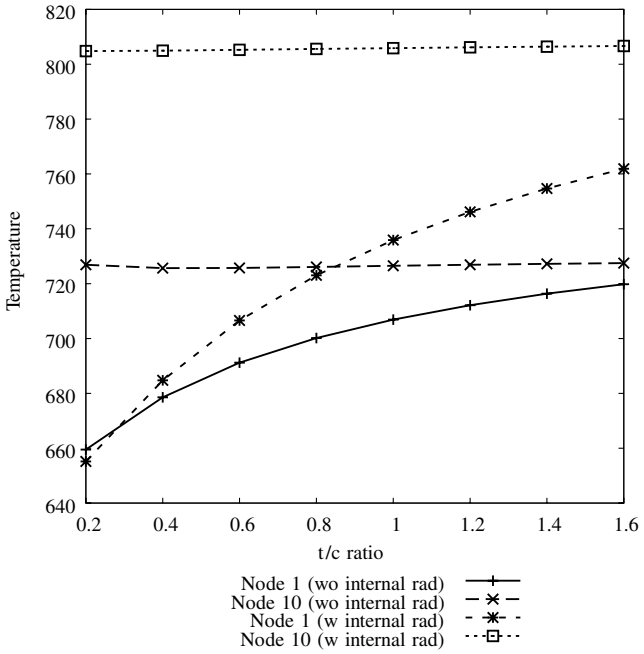

Fig. 5 Parametric temperature variation at nodes 1 and 10: with and without internal radiation.

Wing Box

A wing box under simple thermal and mechanical loading has been analyzed to demonstrate the thermal and thermoelastic capabilities of the new software capability, and the results have been validated against NASTRAN.

The analysis is steady state in nature, where the lower and upper surfaces have a uniform heat flux of 50 kW/m^2 and 2 kW/m^2, respectively. In addition, a uniform pressure load has been applied over the lower surface of the wing. Figure 13 shows the finite element mesh used for the analysis. The thermal model contains a layer of thermal protection system tiles (TPS) of uniform thickness, which are modeled with three-dimensional hexahedral TPS elements. These have not been included in the structural model because they are not part of the primary load-carrying structure. The material properties are listed in Table 1, and the configuration's geometry

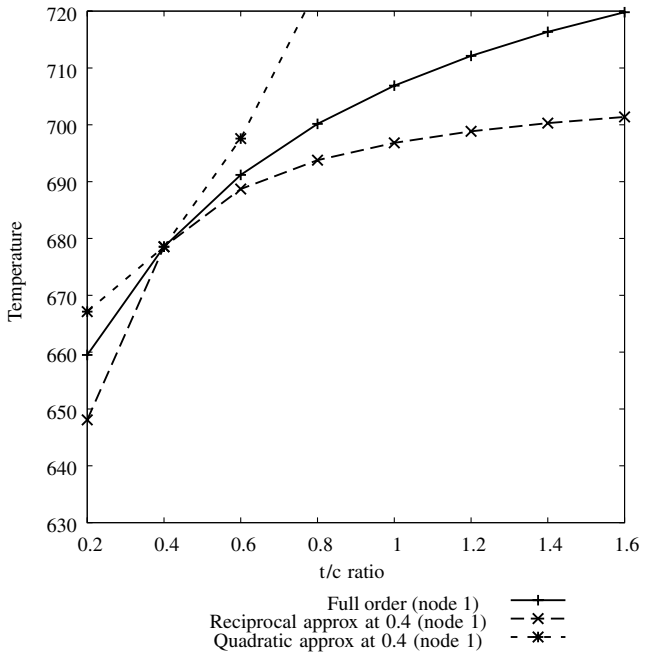

Fig. 6 Cavity nodal temperature approximation from sensitivity analysis of final response at design variable value of 0.4 (node 1).

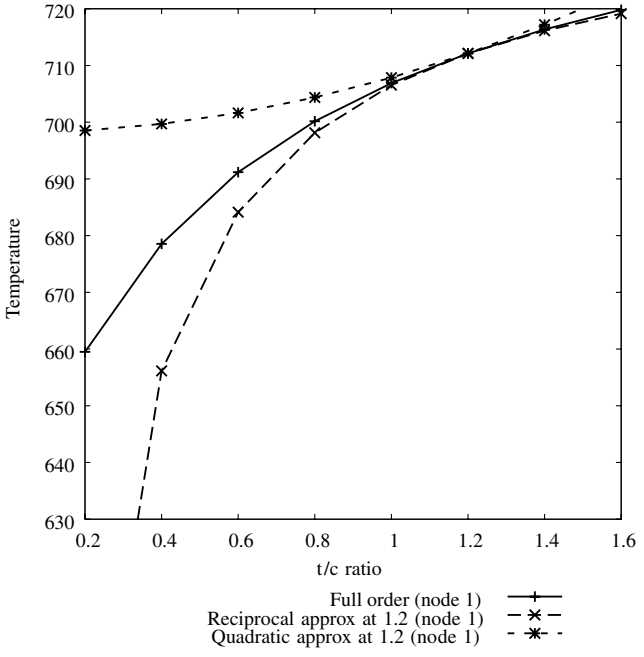

Fig. 8 Cavity nodal temperature approximation from sensitivity analysis of final response at design variable value of 1.2 (node 1).

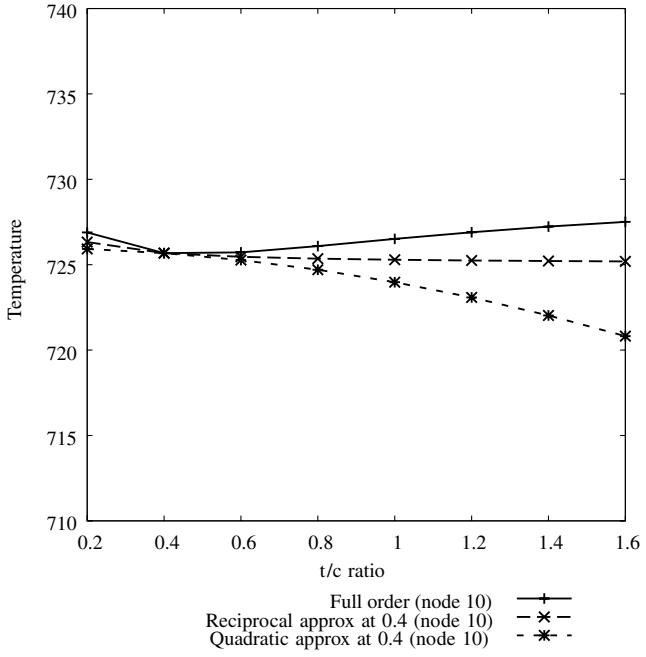

Fig. 7 Cavity nodal temperature approximation from sensitivity analysis of final response at design variable value of 0.4 (node 10).

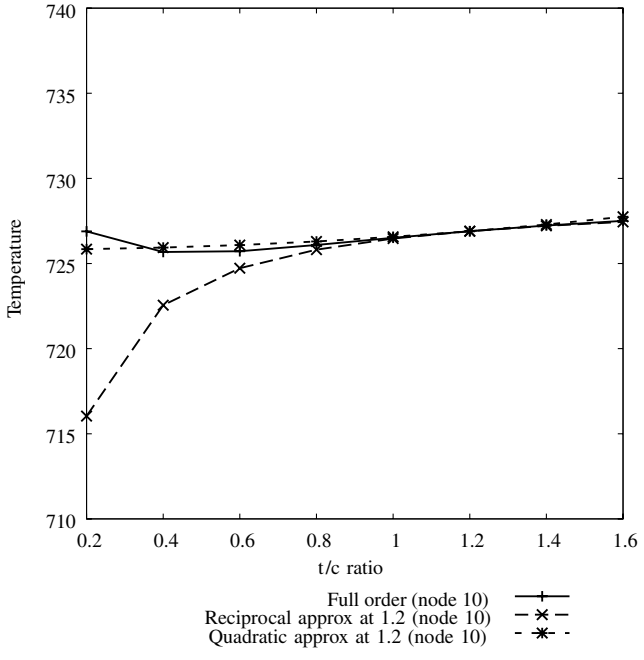

Fig. 9 Cavity nodal temperature approximation from sensitivity analysis of final response at design variable value of 1.2 (node 10).

shape design variables used for creating the wing box geometry are listed in Table 2. The number of nodes and elements for each mesh are listed in Table 3.

Temperature contour plots from thermal analysis are shown in Figs. 14 and 15. TPS layers are excluded from this plot. The figures show that internal radiation leads to a considerable change in the temperature distribution. The wing can lose heat only through radiation from the upper and lower TPS surfaces. Because of the difference in heat flux over the lower and upper wing surfaces, part of the energy from the lower skin is conducted to the upper skin and is lost through radiation from there. Internal radiation provides an additional mode of heat transfer from lower to upper skin and, hence, affects skin temperatures. This effect is dependent upon the absolute value of temperature due to the dependence of radiative flux on fourth power of temperature.

The structural temperatures obtained for this case are very high, because the heat flux values were taken from space shuttle data [1,2] where the problem is transient in nature. However, the motivation here is to demonstrate validity of the new design-oriented numerical capability and its underlying formulation, to study behavior of approximations and computational performance, and to prepare for transient analysis cases, to be reported in subsequent papers. Lower values of surface heat flux could be used to obtain lower steady-state structural temperatures, but will not change the insights and conclusions of the present work.

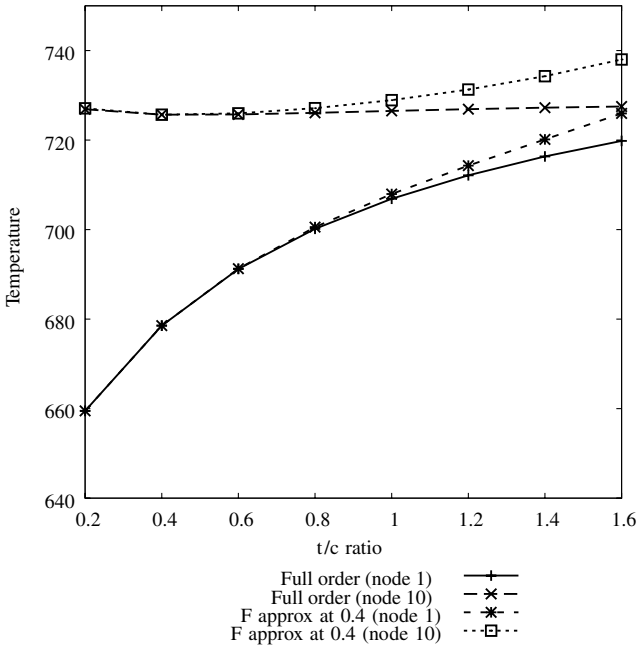

Fig. 10 Cavity nodal temperature using linear approximation of $[F_{i-j}]$ as intermediate response function at design variable value of 0.4 ($[F_{i-j}]$ used as intermediate variable).

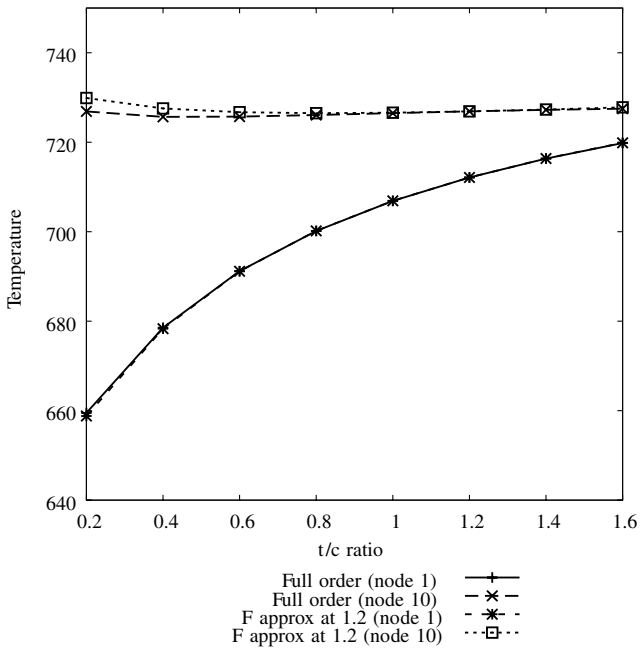

Fig. 11 Cavity nodal temperature using linear approximation of $[F_{i-j}]$ as intermediate response function at design variable value of 1.2 ($[F_{i-j}]$ used as intermediate variable).

Effects of configuration shape variation on the thermoelastic behavior are studied in the next few figures. Figure 16 shows the variation of temperature on nodes 1 and 81 on the lower skin. As shown in Fig. 13, node 1 is located at the root leading edge (LE), and node 81 is located between the second and third ribs from the root and between the first and second spars from the LE. The difference in temperatures due to internal radiation can be clearly seen. Also, it is interesting to note that the temperature at node 81 remains insensitive to the change in LE sweep. A validation of the temperatures at node 81 is shown in Fig. 17.

Figure 18 contains a plot of temperatures obtained from a full nonlinear analysis, but using a Taylor series approximation for $[F]$

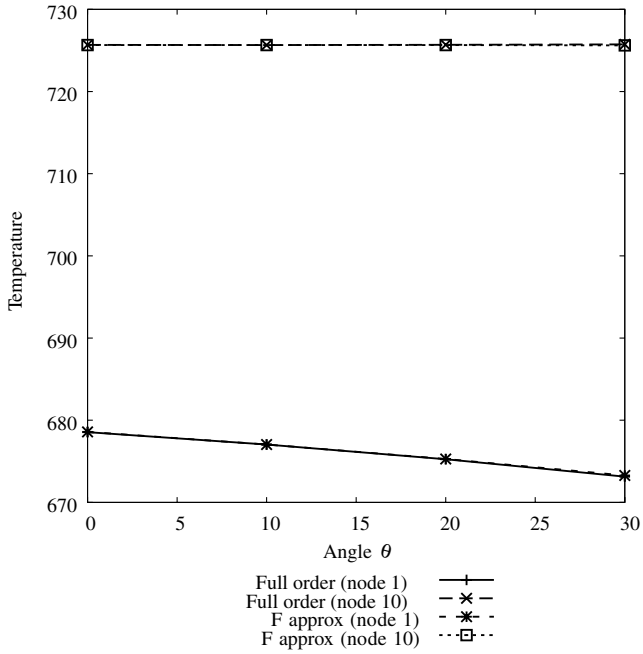

Fig. 12 Cavity temperature approximation using linear approximation of $[F_{i-j}]$ as intermediate response function with shearing angle as design variable ($[F_{i-j}]$ used as intermediate variable).

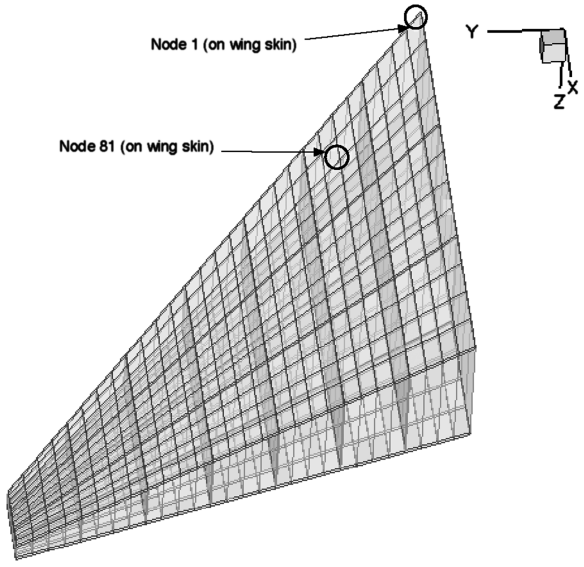

Fig. 13 Wing finite element mesh.

[Eq. (68)]. As can be seen, the results are in very good agreement with the full-order analysis.

Thermoelastic deformation of the wing structure is shown in Fig. 19, and the parametric plot of the wing tip displacement variation with respect to the LE sweep, is shown in Fig. 20. This plot also includes results from NASTRAN and good agreement can be seen between the results from the new FESystem capability and NASTRAN.

Table 2 Wing design variable base values

Design variable	Base value
AR	3.1
Λ_{LE}	43
c_{root}	10.2
c_{tip}/c_{root}	0.16
t_{wing}/c_{root}	0.2

Table 3 Wing structural and thermal finite element mesh details

Mesh	Nodes	Rods	Quads	Hex
Thermal	1508	880	416	672
Structural	754	880	416	——

Finally, variation of typical displacement and stress response functions with sweep angle for the wing box under thermal and mechanical loads is shown in Figs. 21 and 22. Direct, reciprocal, and quadratic approximations are shown. It is important to note the different quality of approximation each type of approximation provides to the different responses: behavior that motivates the usage, in multidisciplinary problems, of approximations that adjust themselves, using proper intermediate design variables and response functions, to each design variable/response function pair separately.

CPU Time Savings

Computational costs of the approximation introduced in the earlier sections (approximating the shape-factor matrix, but still performing the full nonlinear analysis) are presented in Tables 4 and 5.

Table 4 lists the CPU times for calculation of the shape-factor matrix and for the analysis. The CPU times are reported for six

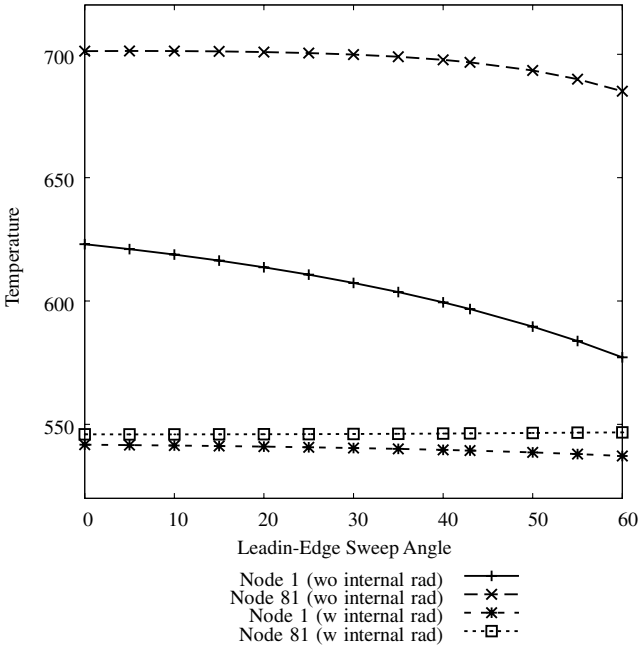

Fig. 16 Wing skin temperature.

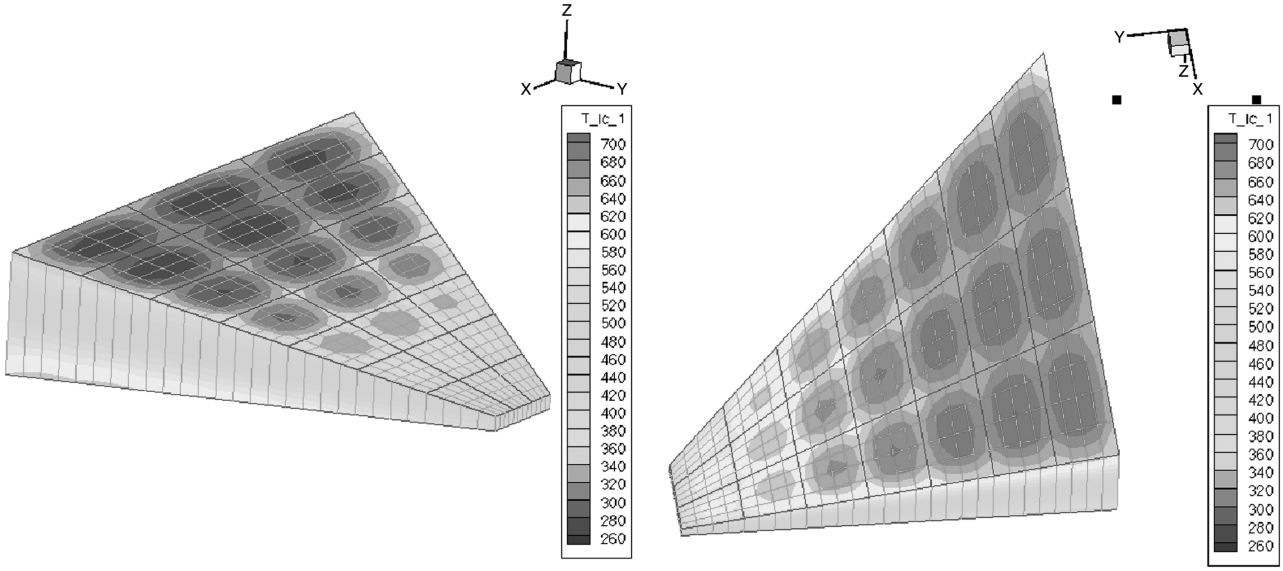

Fig. 14 Temperature contours over upper and lower wing skin: external radiation.

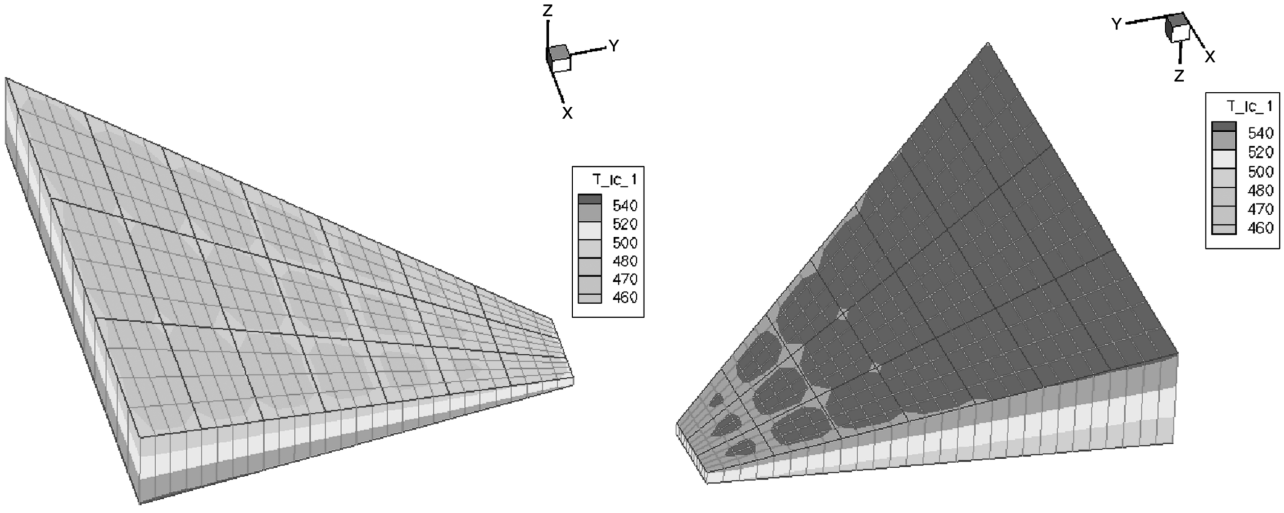

Fig. 15 Temperature contours over upper and lower wing skin: external and internal radiation.

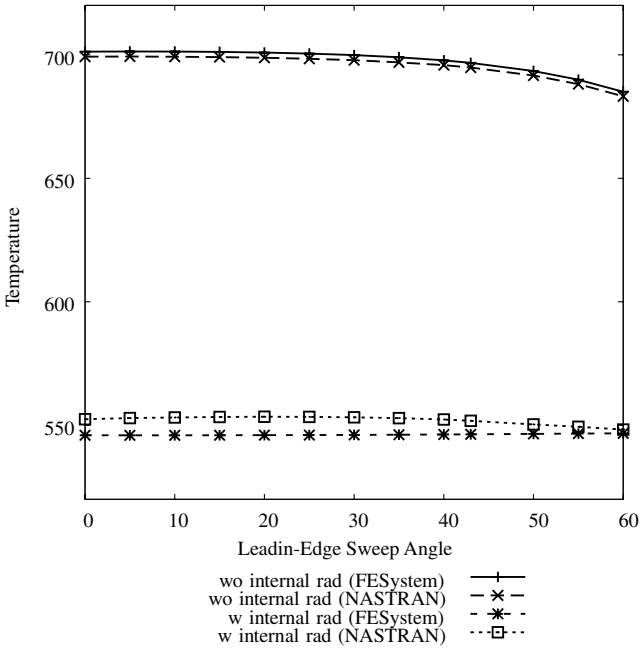

Fig. 17 Wing skin temperature validation against NASTRAN for node 81.

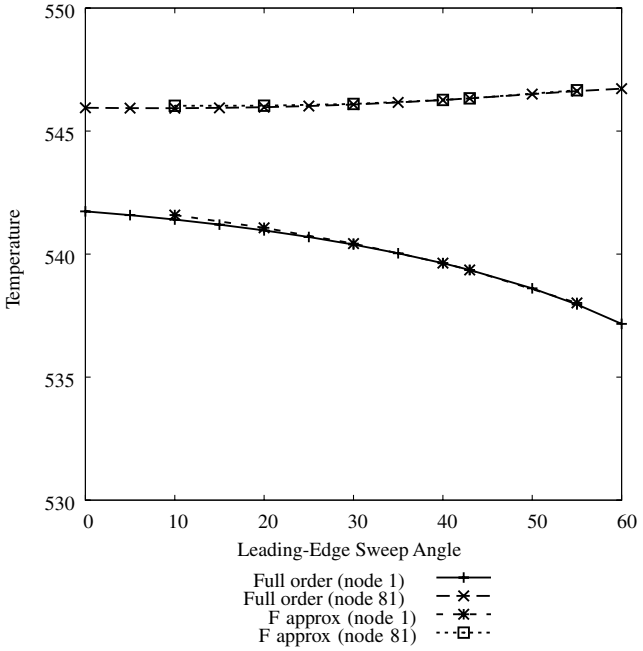

Fig. 18 Wing skin nodal temperature using linear approximation of $[F_{i-j}]$ as intermediate response function for wing leading edge sweep as design variable ($[F_{i-j}]$ used as intermediate variable).

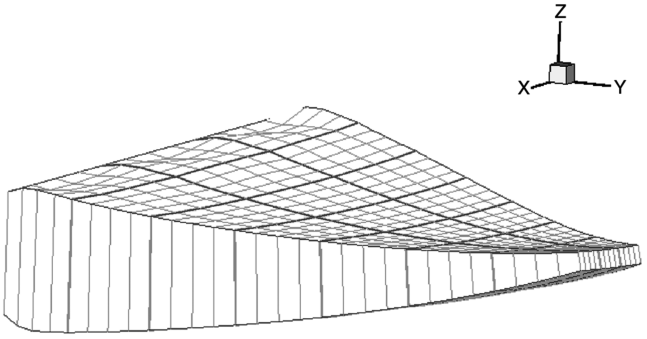

Fig. 19 Deformed mesh due to thermal loads: external and internal radiation (magnification factor = 20.0).

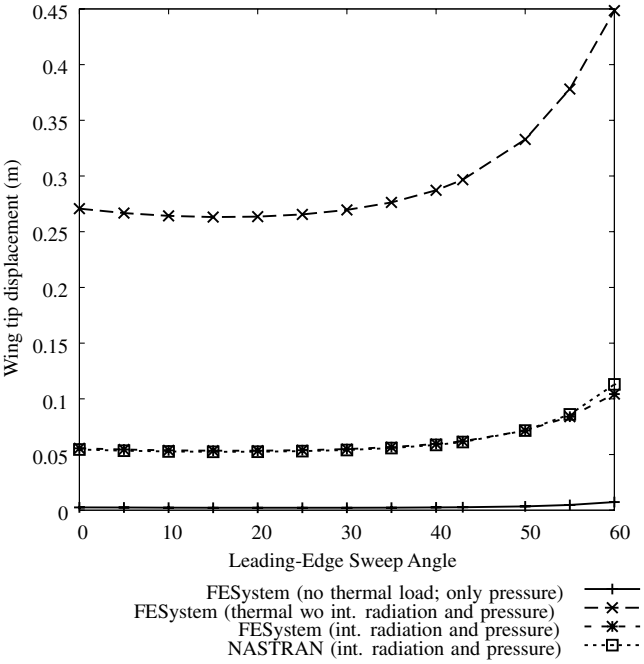

Fig. 20 Wing tip displacement.

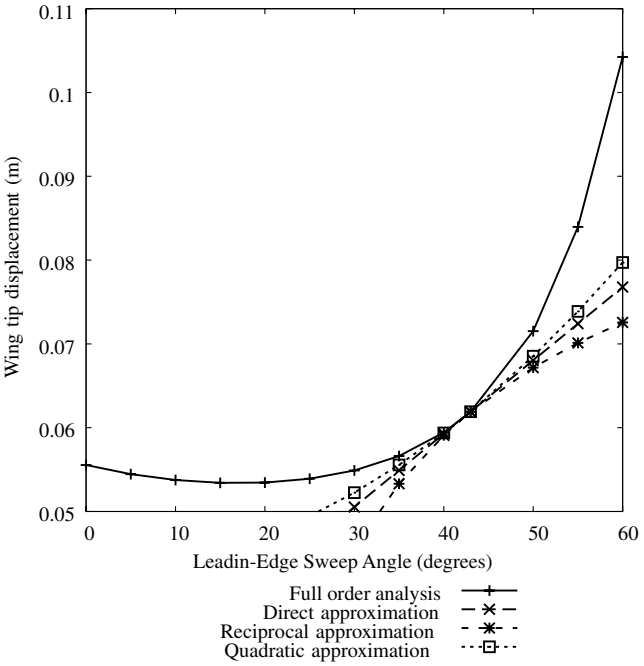

Fig. 21 Wing tip displacement approximation.

different mesh densities. The number of internal cavity radiation surfaces for each mesh, and the number of conduction finite elements, are listed in the first two columns. The third lists the time required for calculation of the shape-factor matrix, and its percentage in terms of the total analysis time (listed in brackets). Column four and five list the total CPU seconds required for analysis and sensitivity analysis, respectively. It can be seen that calculation of shape-factor matrix is a costly process, calling for the use of an efficient approximation. The percentage fraction of this cost with respect to the total analysis cost increases before decreasing again, due to other operations involved in the solution process whose cost rises for higher mesh densities. One such operation is the inversion of the $[B]$ matrix in the radiation problem. It is a dense matrix and, hence, its inversion is costly for larger systems.

Table 4 Analysis times for different thermal finite element mesh densities (all values in seconds, CPU = 1.83 GHz Intel Core Duo, RAM = 1.5 GB 667 MHz DDR2)

No. rad. surfaces per rad. cavity	# Thermal FE (21 cavities)	$[F_{i-j}]$ time	Total analysis time	Total semi-analytic sensitivity time
16	752	0.68 (38.6%)	1.76	2.90
48	2176	5.93 (60.26%)	9.84	18.18
96	4272	22.70 (55.8%)	40.76	65.29
160	7040	60.26 (53.58%)	112.46	187.97
240	10480	131.28 (43.8%)	299.40	466.79

Table 5 CPU time savings of various sensitivity-analysis approaches for different thermal finite element mesh densities (numbers are % savings in CPU time, CPU = 1.83 GHz Intel Core Duo, RAM = 1.5 GB 667 MHz DDR2)

No. rad. surfaces per rad. cavity	Semi-analytic vs finite difference	$[F_{i-j}]$ approx. vs finite difference	$[F_{i-j}]$ approx. vs semi-analytic
16	17.63	38.68	46.96
48	7.64	60.22	65.21
96	19.90	55.68	69.52
160	16.43	53.59	64.12
240	22.05	43.85	56.25

Table 5 lists the percentage CPU comparison with increasing mesh densities for three different approaches to sensitivity analysis: 1) finite difference sensitivity, 2) semi-analytic sensitivity, and 3) semi-analytic sensitivity with $[F_{i-j}]$ approximated. The second column lists the savings of the semi-analytic approach with full calculation of F_{i-j} over the finite difference sensitivity-analysis approach. The second and third columns list the savings due to semi-analytic sensitivity analysis using approximated $[F_{i-j}]$ matrix vs the finite difference and semi-analytic method with full calculation of $[F_{i-j}]$, respectively. Results are listed for the same three mesh densities as in Table 4.

Conclusions

An integrated design-oriented thermostructural capability for the shape optimization of flight vehicles has been described together with supporting analysis, sensitivity analysis, and numerical implementation issues. The work discussed here focuses on the steady-state problem, and addresses conduction finite element and radiation panels mesh-to-mesh information exchange under conditions of changing meshes due to shape variation of the configurations during optimization. The sensitivity of structural responses, dependent on both mechanical and thermal parts of the coupled problem is discussed. Both external and internal radiation are taken into account. Parametric studies of system responses, such as temperature and displacement, are used to validate the sensitivity computations and to assess accuracy of various approximation techniques, including Taylor-series-based approximations in intermediate design variables and an approximation in which radiation shape factors are treated as intermediate response functions to be approximated by Taylor series and then used in full-order nonlinear thermal analysis. Selected results demonstrate the complex nature of dependency of system outputs on system design variables and the need for multipoint approximations when Taylor series approximations are used. Sensitivity-analysis CPU savings results as functions of the density of finite element and radiation meshes used are provided.

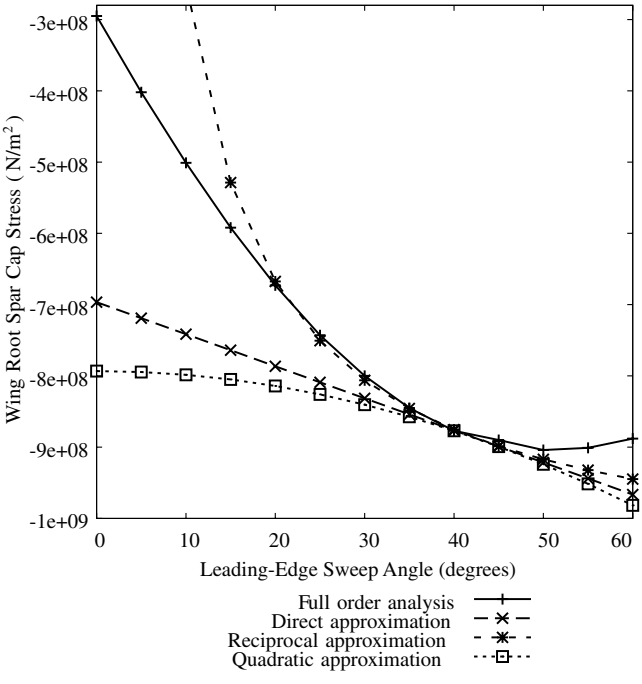

Fig. 22 Wing root stress approximation.

The computational capability developed for this work, and discussed here, offers a level of integration for the coupled shape sensitivity analysis between the thermal and structural parts that is still unavailable with current thermostructural capabilities. The formulation of the design-oriented approach (for shape optimization) of the system's matrices, and insights regarding sensitivity computations, approximations accuracy, and computational costs, lead to the next step: extension of the work to the transient case and the case of temperature dependent materials properties. This follow-up work will be described and discussed in a subsequent paper.

Acknowledgments

This work is supported by a NASA grant as part of the Space Vehicle Technology Institute and the Constellation University Institutes Project. We are grateful for this support.

References

[1] Gong, A., Quinn, R., and Ko, W., "Reentry Heating Analysis of Space Shuttle with Comparison of Flight Data," *Computational Aspects of Heat Transfer in Structures*, NASA CP-2216, 1982, pp. 271–294.

[2] Ko, W., Quinn, R., and Gong, A., "Reentry Heat Transfer Analysis of the Space Shuttle Orbiter," *Computational Aspects of Heat Transfer in Structures*, NASA CP-2216, 1982, pp. 295–326.

[3] Ko, W., Olona, T., and Muamoto, K. M., "Optimum Element Density Studies for Finite Element Thermal Analysis of Hypersonic Aircraft Structures," NASA, TM 4163, 1990.

[4] Ko, W., Quinn, R., and Leslie, G., "Effect of Internal Convection and Internal Radiation on the Structural Temperatures of Space Shuttle Orbiter," NASA, TM 100414, 1988.

[5] Meric, R. A., "Material and Load Optimization of Thermoelastic Solids, Part 1: Sensitivity Analysis," *Journal of Thermal Stresses*, Vol. 9, No. 4, 1986, pp. 359–372. doi:10.1080/01495738608961912

[6] Meric, R. A., "Material and Load Optimization of Thermoelastic Solids, Part 2: Numerical Results," *Journal of Thermal Stresses*, Vol. 9, No. 4, 1986, pp. 373–388. doi:10.1080/01495738608961913

[7] Meric, R. A., "Shape Optimization of Thermoelastic Solids," *Journal of Thermal Stresses*, Vol. 11, No. 3, 1988, pp. 187–206. doi:10.1080/01495738808961932

[8] Tortorelli, D. A., Subramani, G., and Lu, C. Y., "Sensitivity analysis for coupled thermoelastic systems," *International Journal of Solids and Structures*, Vol. 27, No. 12, 1991, pp. 1477–1497. doi:10.1016/0020-7683(91)90073-O

[9] Tortorelli, D. A., Haber, R. B., and Lu, C. Y., "Adjoint Sensitivity Analysis for Nonlinear Dynamic Thermoelastic Systems," *AIAA Journal*, Vol. 29, No. 2, Feb. 1991, pp. 253–263.

[10] Dems, K., and Korycki, R., "Sensitivity Analysis and Optimum Design for Steady Conduction Problem with Radiative Heat Transfer," *Journal of Thermal Stresses*, Vol. 28, No. 2, 2004, pp. 213–232.

[11] Gu, Y., Chen, B., Zhao, H., Zhang, H., and Grandhi, R. V., "Optimization and Sensitivity Analysis of Thermal Structures Coupled with Heat Transfer," *Structural and Multidisciplinary Optimization* (submitted for publication).

[12] Gu, Y., Chen, B., Zhang, H., and Grandhi, R. V., "Sensitivity Analysis Method for Linear and Nonlinear Transient Heat Conduction with Precise Time Integration," *Structural and Multidisciplinary Optimization*, Vol. 24, No. 1, Aug. 2002, pp. 23–37.

[13] van Keulen, F., Haftka, R., and Kim, N., "Review of Options for Structural Design Sensitivity Analysis, Part 1: Linear Systems," *Computer Methods in Applied Mechanics and Engineering*, Vol. 194, Nos. 30–33, Aug. 2005, pp. 3213–3243. doi:10.1016/j.cma.2005.02.002

[14] Chen, B., Gu, Y., Zhang, H., and Zhao, G., "Structural Design Optimization on Thermally Induced Vibration," *International Journal for Numerical Methods in Engineering*, Vol. 58, No. 8, Oct. 2003, pp. 1187–1212. doi:10.1002/nme.814

[15] Xu, S., and Grandhi, R. V., "Structural Optimization with Thermal and Mechanical Constraints," AIAA Paper A98-39901, 1998.

[16] Kirk, B., Peterson, J. W., Stogner, R. H., and Carey, G. F., "libMesh: A C++ Library for Parallel Adaptive Mesh Refinement/Coarsening Simulations," *Engineering with Computers*, Vol. 22, Nos. 3–4, 2006, pp. 237–254, http://libmesh.sourceforge.net.

[17] Balay, S., Buschelman, K., Gropp, W. D., Kaushik, D., Knepley, M. G., McInnes, L. C., Smith, B. F., and Zhang, H., "PETSc Web page," 2001, http://www.mcs.anl.gov/petsc.

[18] Balay, S., Buschelman, K., Gropp, W. D., Kaushik, D., Knepley, M. G., McInnes, L. C., Smith, B. F., and Zhang, H., "PETSc Users Manual," Argonne National Lab., TR ANL-95/11: Rev. 2.1.5, 2004.

[19] Thornton, E. A., *Thermal Structures for Aerospace Applications*, AIAA, Reston, VA, 1996.

[20] Haftka, R. T., and Gurdal, Z., *Elements of Structural Optimization*, 3rd ed., Kluwer Academic, Norwell, MA, 1992.

[21] Walton, G. N., "Calculation of Obstructed View Factors by Adaptive Integration," National Inst. of Standards and Technology, TR 6925, 2002.

[22] Schroder, P., and Hanrahan, P., "A Closed Form Expression for the Form Factor Between Two Polygons," Dept. of Computer Science, Princeton Univ., TR CS-TR-404-93, 1993.

[23] Siegel, R., and Howell, J. R., *Thermal Radiation Heat Transfer*, 3rd ed., Hemisphere, New York, 1992.

B. Balachandran
Associate Editor